Confinement effects on the electronic and vibronic properties of $CdS_{0.65}Se_{0.35}$ nanoparticles grown by thermal annealing

Prabhat Verma[a)]
Department of Electronics and Information Science, Kyoto Institute of Technology, Kyoto 606-8585, Japan

Lalita Gupta, S. C. Abbi, and K. P. Jain
Department of Physics, Indian Institute of Technology, New Delhi 110 016, India

(Received 20 January 2000; accepted for publication 27 June 2000)

$CdS_{0.65}Se_{0.35}$ nanoparticles are grown in a glass matrix by thermally annealing a base glass material, in which Cd, S, and Se were introduced by diffusion. The starting base material contains no crystalline structure. A comparative study of the confinement effects on the annealed samples using photoluminescence, low-frequency Raman, and optical Raman scattering experiments is presented. Growth of nanoparticles is observed with the three independent experimental techniques as the annealing temperature is varied from 550 to 800 °C. Radii of the thermally grown nanoparticles calculated from the three independent techniques are found to be in good agreement. In addition, surface phonon modes are observed in the optical spectral range, the frequencies of which agree well with those calculated theoretically. As expected from the theory, the positions of the surface phonons are found to be independent of the particle size. © *2000 American Institute of Physics.* [S0021-8979(00)09419-6]

I. INTRODUCTION

Recently, the optical and electronic properties of semiconductor nanostructures have attracted great interest,[1–19] because they differ strongly from those of the corresponding bulk material, exhibiting a wide range of size-dependent properties. A good review on this subject can be found in Ref. 3. Semiconductor nanoparticles embedded in solid matrices have been studied particularly extensively[11–19] from the fundamental point of view as well as for application to optical processing devices. Semiconductor particles with diameters of a few nanometers typically contain several hundreds to several thousands of atoms, yet are too small to have bulk electronic properties. In a small nanocrystal with size comparable to the Bohr radius of the corresponding bulk material, spatial confinement effects on the electron–hole system and on the propagation of phonons become significant. Theoretical models predict[1] that the energy spectrum of such a material consists of a series of discrete lines, which change their positions with particle size, and a blueshift in the absorption edge with respect to the corresponding bulk material is observed. This blueshift in the band gap gives a measure of the confinement, which can be observed in absorption spectroscopy[2] or photoluminescence[1] (PL) experiments.

Raman scattering, which is significantly influenced by surface conditions, particle size, and the size distribution of a nanoparticle system, is one of the best nondestructive techniques to obtain information about the electronic and vibronic states in a confined system. Confinement of phonons within a small nanoparticle results in quantization of $\mathbf{q}$, leading to interesting changes in the vibrational spectrum. Due to this confinement, the $\mathbf{q}=0$ selection rule is relaxed and, hence, low-frequency acoustic phonons, known as confined acoustic phonons, are observed in Raman spectra,[15–18] the energies of which depend strongly on the particle size. In previous studies,[15–19] a peak in the low-frequency range was observed in Raman scattering from acoustic vibrations of these spherical particles, and the particle size was deduced from the energy of this peak. However, in a recent study,[14] it was shown that two types of confined acoustic phonons, namely, polarized and depolarized phonons, are observed in low-frequency Raman scattering. Optical phonons observed in Raman spectra are also influenced by the confinement effects in a nanoparticle system. The peak positions of optical phonons shift to low energy and the phonons are asymmetrically broadened compared to the bulk phonons.[20] Additionally, since the surface-to-volume ratio is large for small particles, the surface phonon modes (SM) become prominent in a nanoparticle system. These can be observed in the optical spectral range in Raman spectra.

Recently, a considerable amount of work has been reported[14–24] on the study of optical properties of commercially available sharp-cut color filters, in which CdS_xSe_{1-x} nanoparticles are embedded in a glass matrix. However, at present, information on the fundamental physical properties of such a system is still insufficient, and much more information and knowledge are required in order to use them as optical processing devices. It is critical to have an accurate knowledge of the particle size and the size distribution in order to use them in the field of nonlinear optics. In this article, we present a systematic spectroscopic study on $CdS_{0.65}Se_{0.35}$ nanoparticles of various sizes, which are thermally grown in a glass matrix. It is the purpose of this article to present a comparative study of PL and Raman scattering on nanoparticles with a view to understand the effects of

a)Electronic mail: verma@dj.kit.ac.jp

localization on the electronic and vibronic properties of the confined system. A comparison of the confinement effects in PL, low-frequency Raman scattering, and optical Raman scattering studies, shows good agreement between the three independent techniques used to study the confinement effects. Considering the case of strong confinement[25] of the electron–hole system, confinement energy has been calculated for nanoparticles as a function of their sizes. A comparison of the calculation with the experimental values of the confinement energies, measured from the shift in the band-edge luminescence, enables us to estimate the particle size in the thermally grown nanoparticle system. Confined acoustic phonons, which are observed very close to the laser line in the low-frequency Raman scattering experiments, have been successfully measured in both polarized and depolarized configurations. Using a theoretical model[14] recently presented by one of the present authors, the particle sizes have been calculated from the frequency positions of the confined acoustic phonons. Further, confinement effects have been studied in detail for the first-order optical phonons. Due to the spatial localization of the phonon correlation function in a nanoparticle system, the line shapes of the optical phonons are greatly modified and the phonons exhibit softening accompanied by an asymmetric broadening. This phenomenon has been discussed using the spatial correlation model[26–28] and the particle sizes have been obtained from the estimated correlation lengths. The particle sizes obtained from the three independent channels, namely, luminescence, confined acoustic phonons, and optical phonons, are found to be in excellent agreement. It is also demonstrated that the asymmetry in the LO phonons accounts well for the confinement and the particle size can be estimated from the same. In addition, the surface phonon modes are also observed at frequencies slightly below the frequencies of the LO phonons. Calculations show that the surface phonon frequencies are independent of the particle size.[29] The observed surface phonon frequencies are found to be in good agreement with the calculated ones, and they are indeed particle-size independent.

II. EXPERIMENTAL DETAILS

The base material used in the present work contains a glass matrix in which Cd, S, and Se were introduced by diffusion. This is a commercial material, procured from Schott Inc., Germany. This base material, which contains no semiconducting structure, was annealed at various temperatures ranging from 550 to 800 °C for a period of 2 h in an electric furnace, and CdS_xSe_{1-x} nanoparticles were thermally grown in the glass matrix. The size of the grown particles depended on the annealing temperature. The color of the samples changes from yellow to deep orange when the annealing temperature is increased. The composition x in the mixed crystal of CdS_xSe_{1-x} depends upon the initial ratio of S and Se in the base material, and is 0.65 for the present case. The samples thus obtained were characterized by PL and Raman scattering experiments.

All experiments were performed at room temperature in backscattering geometry employing a Jobin–Yvon double monochromator with low laser power density to ensure that there were no changes in the optical properties of the samples due to laser illumination. Raman scattering was detected using a charge-coupled-device detector, where as PL measurements were performed with a photomultiplier tube and a photon-counting system. Raman scattering in the optical spectral range and PL experiments were performed with the 488 nm line of an Ar-ion laser. In order to avoid luminescence background near the laser line, low-frequency Raman scattering experiments were performed much below the band gap using the 850.8 nm wavelength of a Ti–sapphire laser pumped by an Ar-ion laser. The accuracy in the measurements was about 0.3 cm^{-1} for $\lambda = 488$ nm and about 0.1 cm^{-1} for $\lambda = 851$ nm.

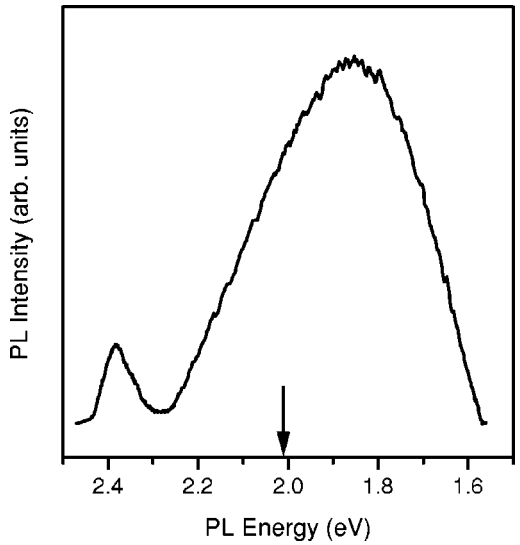

FIG. 1. Room-temperature PL spectrum from the sample annealed at 550 °C. The band-edge luminescence around 2.38 eV indicates that the crystalline structure in the sample has started growing at 550 °C. The broad structure around 1.86 eV is from deep traps. The arrow at 2.01 eV points to the band-edge position of the corresponding bulk. A large blueshift of the PL peak from the bulk band edge indicates that the grown nanoparticles have a small size.

III. RESULTS AND DISCUSSION

A. Photoluminescence

Figure 1 presents room-temperature PL spectra for the sample annealed at 550 °C, showing two luminescence structures around 2.38 and 1.86 eV, respectively. The first structure corresponds to recombinations at the band edge and from very shallow states close to the conduction band. This structure shows an asymmetric tail on the low-frequency side, indicating that the luminescence includes transitions from some lower states very close to the conduction band. These are very shallow defect levels nearly degenerate with the conduction band, normally observed in room-temperature PL from nanostructured materials. Due to the presence of these shallow levels, the PL line shape is modified and the peak position does not give the accurate value of the band edge. Therefore, one must consider the uncertainty in band-edge estimation from the extent of the low-frequency tail. Taking this uncertainty into account, the nanoparticle band

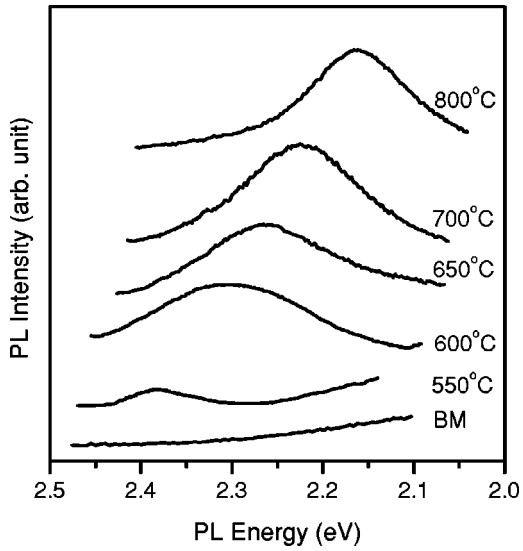

FIG. 2. PL structure corresponding to the band edge from samples annealed at the indicated temperatures. The shift in the PL peak shows increase of particle size with increasing annealing temperature. For comparison, a PL spectrum from the unannealed base material (BM) is also presented.

edge, as determined from Fig. 1, is 2.38 ± 0.02 eV. In the following discussion, we will focus our attention on this structure. The second structure in Fig. 1, which appears in the form of a broadband, corresponds to radiative recombinations associated with deep traps. The origin of traps can, in general, be related either to the surface states, or to the impurity and defect states within the nanoparticles.

The peak position of the first structure in Fig. 1 is blueshifted with respect to the corresponding bulk material due to the confinement energy. Assuming a linear variation of the band gap with respect to the composition x in CdS_xSe_{1-x} bulk material, the band gap of the corresponding bulk material for this sample ($x=0.65$) should be 2.01 eV (indicated by the arrow in Fig. 1). This implies that the blueshift in the band-edge luminescence in this sample due to the confinement is about 370 ± 20 meV. As the annealing temperature is increased, this PL structure gets stronger and shifts towards the low-energy side, i.e., towards the bulk band edge. Figure 2 shows this PL structure for samples annealed at various temperatures ranging from 550 to 800 °C. For comparison, a PL spectrum from the unannealed base material is also presented in Fig. 2, which shows no luminescence peak, indicating that there is no crystalline structure present in the base material. As evident from Fig. 2, this luminescence structure shifts to the low-energy side with increasing annealing temperature, indicating a change in the band gap, which is also evident from the visible change in the color of the annealed samples.

Increase in the fundamental band gap of a nanostructured material due to confinement effects is well established. The effect of confinement on the exciton motion becomes pronounced as particle size decreases. At very small particle sizes (comparable to the Bohr radius), the character of the exciton starts disappearing and the electrons and holes become individually confined, because the kinetic energies of the electrons and holes become dominant and the Coulomb interaction between electrons and holes starts losing its significance. This results in a positive confinement energy and the band edge of the nanocrystal is blueshifted with respect to the corresponding bulk material. As a consequence, the luminescence corresponding to the band edge appears at a higher energy. The shift in the luminescence peak with increasing annealing temperature in Fig. 2 indicates the growth of semiconducting nanoparticles as the annealing temperature is increased from 550 to 800 °C. The size of these thermally grown nanoparticles can be estimated from the blueshift in the band edge with respect to the bulk band edge using existing models. In the present study, we have used the model given by Kayanuma,[25] where a variational calculation is presented for the band-gap energy of a confined system giving good approximation to the exact energy gaps. We expect small particles in our samples and will, therefore, use the case of strong confinement discussed by Kayanuma. According to this model, the lowest energy of an electron–hole pair in a strongly confined system is given by

$$E = E_g + \frac{\hbar^2}{2\mu}\left[\frac{\pi}{R}\right]^2 - 1.786\,\frac{e^2}{\epsilon R} - 0.248E^*_{\mathrm{Ry}}, \tag{1}$$

where E_g is the band-gap energy of the bulk material, μ is the reduced mass, R is the particle radius, e is the electron charge, ϵ is the high-frequency dielectric constant of the material, and $E^*_{\mathrm{Ry}}=(\mu e^4/2\epsilon^2\hbar^2)$ is the effective Rydberg energy. Considering the effective Rydberg for the unit of energy and the effective Bohr radius, $a^*_B=(\epsilon\hbar^2/\mu e^2)$, for the unit of length, the energy shift in Eq. (1) can be expressed as

$$\varepsilon(\sigma,\rho)=\left(\frac{\pi}{\rho}\right)^2 - \frac{3.572}{\rho} - 0.248, \tag{2}$$

where $\varepsilon=(E-E_g)/E^*_{\mathrm{Ry}}$ is the normalized energy shift, $\sigma=m_h/m_e$, m_h, and m_e, being hole and electron masses, respectively, and $\rho=R/a^*_B$ is the normalized radius.

With $m_e=0.12$, $m_h=0.4$, and $\epsilon=5.32$ for CdS and $m_e=0.18$, $m_h=0.6$, and $\epsilon=6.1$ for CdSe,[30,31] we get $E^*_{\mathrm{Ry}}=47$ meV and $a^*_B=27$ Å for $CdS_{0.65}Se_{0.35}$ nanocrystals by taking a linear interpolation of the physical quantities between $x=0$ and $x=1$. Taking care of the units in Eq. (1), e^2 was replaced by $e^2/4\pi$, and μ and ϵ were expressed in the units of the electron mass and the dielectric constant of vacuum, respectively. Using the PL peak position as the band edge, we estimated the particle size for various annealing temperatures from Eq. (2). This calculation may not give an accurate value of the particle size, because the PL position may not give an accurate value of the band edge. We, therefore, estimated an error in the size calculation for each annealing temperature from the asymmetric tail of the luminescence band. The particle sizes estimated from Eq. (2) are listed in Table I (under the column $R1$), along with the corresponding annealing temperatures and the luminescence energies. An increase in nanoparticle size from 2.8±0.1 to 4.7±0.5 nm with increase in annealing temperature can be observed in Table I.

Although size estimation using PL experiments alone may not give a very reliable value of the particle size, we

TABLE I. The experimental values obtained for samples annealed at various temperatures. Annealing temperatures are given under the column T; Band edge indicates the peak position of the band-edge luminescence; $R1$ is the radius of the nanoparticles calculated from PL experiments; $\omega 1$ and $\omega 2$ indicate the frequencies of the depolarized- and the polarized-confined acoustic phonons, respectively; $R2$ is the radius of the nanoparticles calculated from low-frequency Raman scattering experiments; LO1 and LO2 indicate the frequencies of the CdSe-like and CdS-like LO phonons, respectively; $R3$ is the radius of the nanoparticles calculated from the optical phonons; and SM1 and SM2 are the frequency positions of the surface phonon modes associated with LO1 and LO2, respectively.

T (°C)	Band edge (eV)	$R1$ (nm)	$\omega 1$ (cm^{-1})	$\omega 2$ (cm^{-1})	$R2$ (nm)	LO1 (cm^{-1})	LO2 (cm^{-1})	$R3$ (nm)	SM1 (cm^{-1})	SM2 (cm^{-1})
550	2.38±0.02	2.8±0.1	20.2	46.0	2.8	195.0	294.5	2.7	189.0	279.5
600	2.30±0.03	3.2±0.2	19.0	40.2	3.3	195.8	295.2	3.0	189.2	279.8
650	2.26±0.04	3.5±0.3	17.0	37.8	3.5	196.5	296.0	3.4	189.5	280.0
700	2.22±0.03	3.9±0.4	14.8	34.0	3.9	197.2	296.8	3.8	189.5	280.2
750	2.18±0.03	4.5±0.5	13.2	28.8	4.4	198.0	297.5	4.4	189.2	280.0
800	2.17±0.03	4.7±0.5	12.0	26.2	4.8	198.5	298.0	4.8	189.5	280.0

will show later that, when compared with Raman scattering experiments, it gives a good account for relative changes in the particle size.

B. Raman scattering

1. Confined acoustic phonons

Confined acoustic vibrations in nanoparticles are usually described as the eigenfrequencies of a homogeneous elastic sphere under stress-free boundary conditions,[32] and are classified into two categories, torsional and spheroidal, the torsional modes being Raman inactive. These modes can be classified according to the symmetry group of the sphere by the angular quantum number l (=0, 1, 2,...), along with another index p (=1, 2, 3,...), which gives overtones in Raman spectra. The spheroidal modes with $l=0$ and $l=2$ are the only Raman active modes,[33] the former being polarized and the latter depolarized for spherical nanoparticles. This problem was studied in the past[15–19] for semiconducting nanoparticles embedded in a glass matrix, where only one structure in the low-frequency range was observed and no specific polarization properties were reported. Recently, a detailed study was reported[14] on the confined acoustic vibrations in a commercially available series of filter glasses. In Ref. 14, a theoretical model was presented, which established a relation between the particle size, the frequencies, and the widths of various confined acoustic phonons, taking into account the matrix influence on the vibrational spectrum and on its damping. According to this model, the relation between the particle size and the frequency of the polarized-confined acoustic phonon can be established from[14]

$$\sin(\xi)=4n_{\mathrm{eff}}^2 j_1(\xi), \tag{3}$$

with a complex argument

$$\xi=R(\omega+i\Gamma)/v_l, \tag{4}$$

where ω and Γ are the phonon frequency and width, respectively, for the polarized-confined acoustic phonon of the first order, and R is the radius of the nanoparticle. The term $j_1(\xi)$ is the spherical Bessel function of the first kind with order one, v_l is the longitudinal sound velocity in the nanoparticle, and n_{eff} is an effective internal acoustic index given by

$$n_{\mathrm{eff}}^2=n_p^2-f\left[n_m^2-\frac{1}{4}\frac{(\kappa\xi)^2}{1-i(\kappa\xi)}\right], \tag{5}$$

where n_p and n_m are the ratios of transverse-to-longitudinal sound velocities in the particle and in the matrix, respectively, κ is the ratio between the longitudinal sound velocities in the particle and in the matrix, and f is a coupling constant between the particle and the matrix, given by

$$f=\left(\frac{1}{\kappa}\right)^2\frac{\rho_m}{\rho_p}, \tag{6}$$

with ρ_m and ρ_p being the mass densities for the matrix and for the particle, respectively. By substituting n_{eff} from Eq. (5) into Eq. (3), the relation between particle radius R and the phonon frequency ω can be obtained from the real part of Eq. (4).

Low-frequency Raman spectra from the sample annealed at 800 °C are presented as an example in Fig. 3, where curves (a) and (b) correspond to polarized and depolarized configurations, respectively. For comparison, an unpolarized

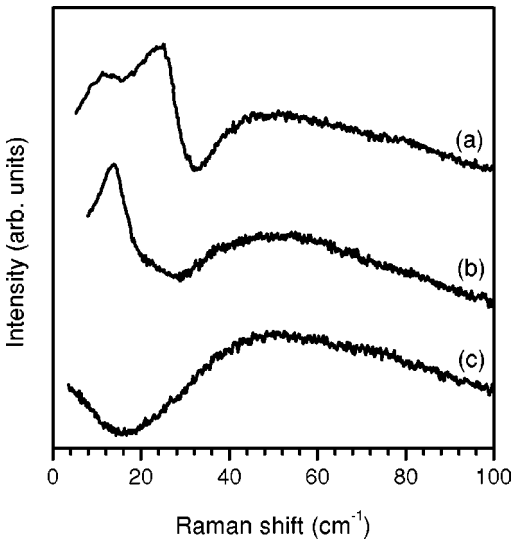

FIG. 3. Low-frequency Raman spectra from the sample annealed at 800 °C. Curves (a) and (b) are polarized and depolarized spectra, respectively, and curve (c) is an unpolarized spectrum from the unannealed base material.

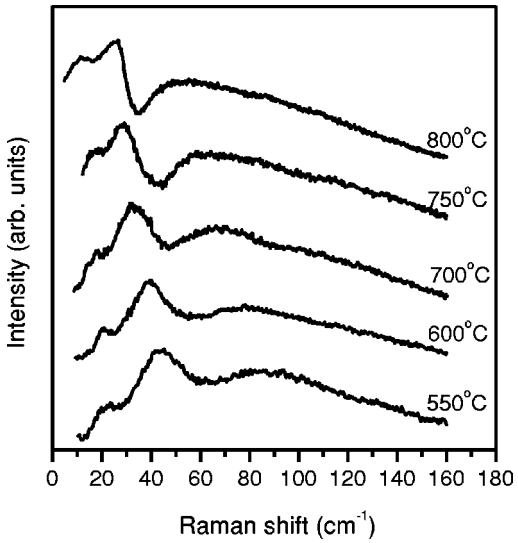

FIG. 4. Polarized low-frequency Raman spectra from samples annealed at the indicated temperatures. Shifts in frequencies of the confined acoustic phonons indicate increase of particle size with annealing temperature.

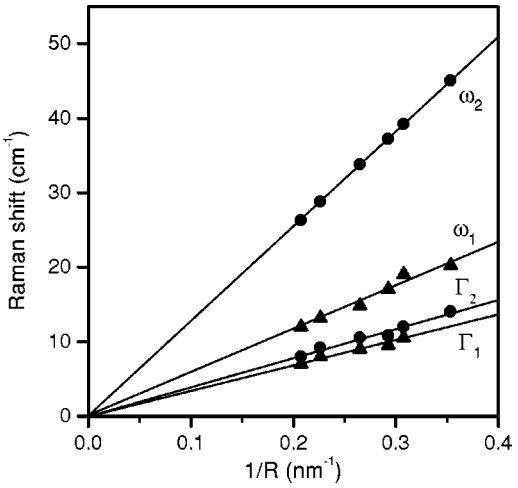

FIG. 5. Linear dependence of the frequencies ω_1 and ω_2 and the linewidths Γ_1 and Γ_2, for the depolarized- and the polarized-confined acoustic phonons, respectively, on $1/R$. The circles and the triangles show experimental points. The straight lines for ω_2 and Γ_2 are obtained from Eq. (4) and those for ω_1 and Γ_1 are linear fits to the experiment.

Raman spectrum from the unannealed base material is presented as curve (c), which shows a broad structure attributed to the vibrations of the glass matrix at about 50 cm^{-1}, known as the Boson peak. The spectra in Fig. 3 have been normalized to this structure, which is also present in curves (a) and (b). Apart from this broad structure, two sharp peaks can be seen at 12 and 26.2 cm^{-1} in curve (a), which correspond to the depolarized- and polarized-confined acoustic vibrations of the nanoparticles, respectively. Curve (b) shows only one peak at 12 cm^{-1}, because the polarized phonon is not observed in the depolarized configuration. Similar results have been observed for other samples annealed at various temperatures and these are presented in Fig. 4 for the parallel polarization configuration. The spectra in Fig. 4 are arranged in the order of increasing annealing temperature. It can be seen from Fig. 4 that the scattering intensities increase and the energies of the confined acoustic phonons decrease with increasing annealing temperature. In order to obtain true values of the phonon energies, a deconvolution was performed after subtracting the base material spectrum [curve (c) in Fig. 3] from each spectrum. The positions of both polarized and depolarized acoustic phonons for samples annealed at various temperatures are listed in Table I. Particle radius R was calculated from Eqs. (3) and (4) by using the experimental values of the frequencies of the polarized-confined phonons. The results are listed in Table I, under the column $R2$.

Equation (4) indicates that the polarized phonon frequency ω and linewidth Γ are inversely proportional to the particle radius R. It has been demonstrated numerically in Ref. 14 that the depolarized phonon modes also follow the same dependence. The experimental values of the frequencies and the linewidths of the polarized and the depolarized phonons obtained from the low-frequency Raman spectra are presented in Fig. 5, which shows a linear dependence of frequencies and linewidths on $1/R$. The straight lines for the polarized phonon frequency (ω_2) and the linewidth (Γ_2) are obtained from Eq. (4). The other two lines for the depolarized phonons are linear fits.

As seen from both PL and low-frequency Raman scattering experiments, the base material shows no evidence of crystalline structure in the glass matrix. After annealing at 550 °C for 2 h, an indication of the growth of nanocrystalline structure can be observed in both experiments. However, at lower annealing temperatures, no growth of nanoparticles could be observed in either experiments. When annealed for a period shorter than 2 h, the particle-size distribution was large, as observed from the large widths of the luminescence band as well as of acoustic phonons (not shown here). An increase in particle size is observed with increasing annealing temperature in both experiments. It can be seen from Table I that the particle sizes calculated from two independent techniques, namely, PL and low-frequency Raman scattering experiments, are in good agreement for all annealing temperatures.

2. Optical and surface phonons

Figure 6 presents a typical Raman spectrum in the optical spectral range from the sample annealed at 800 °C. CdS_xSe_{1-x} material is classified among the so-called ''two-mode behavior alloys,'' which show the simultaneous presence of optical phonons corresponding to CdS and CdSe. The outstanding peaks marked as LO1 at 198.5 cm^{-1} and LO2 at 298 cm^{-1} in Fig. 6 are attributed to the CdS- and CdSe-like LO phonons. Scattering by TO phonons is absent. The second-order spectrum consist of overtones at 396 and 596 cm^{-1}, a combination mode LO1+LO2 at 494 cm^{-1}, and LO2−LO1 at about 100 cm^{-1}. The second-order Raman spectrum reveals that the scattering via Fröhlich interaction[34] is prevailing, because scattering from TO phonons remains absent even in the second-order spectrum. A prominent rise in intensity of combined modes, which is observed for the LO1+LO2 mode in Fig. 6, is common to multimode systems and has been observed previously.[35]

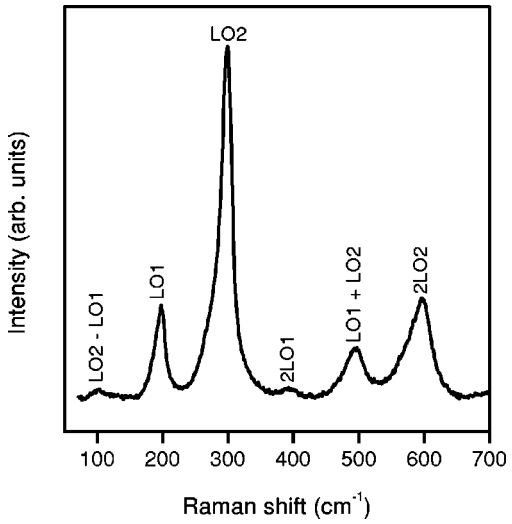

FIG. 6. Optical Raman spectrum from the sample annealed at 800 °C, showing both first- and second-order optical phonons.

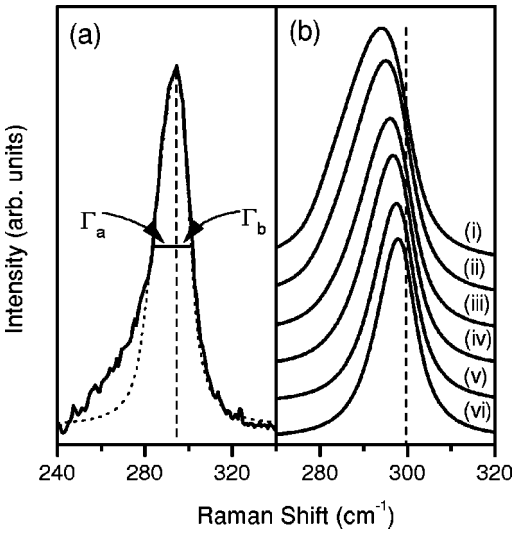

FIG. 7. (a) CdS-like LO phonon for the sample annealed at 550 °C. The dotted curve is a fit obtained from Eq. (7). Γ_a and Γ_b are the half widths on the low-frequency side and the high-frequency side, respectively, of the LO phonon. (b) Theoretical fits obtained from Eq. (7) for the CdS-like LO phonon in Raman spectra from samples annealed at 550, 600, 650, 700, 750, and 800 °C in curves (i)–(vi), respectively. The dashed line indicates the position of the CdS-like LO phonon in corresponding bulk material.

Assuming a linear shift in the LO phonon frequency with respect to the composition x, the positions of LO1 and LO2 phonon modes in bulk CdS_xSe_{1-x} with $x=0.65$ should be 200 and 299.5 cm^{-1}, respectively. The peak positions of LO1 and LO2 modes in Fig. 6 are shifted towards low energy compared to the bulk phonon energies by about 1.5 cm^{-1}. This shift increases to about 5 cm^{-1} for the samples annealed at low temperatures (Table I). Apart from this shift, the LO phonons also show asymmetry which appear as a shoulder-like structure on the low-energy side. The shift and asymmetry in LO phonons arise due to the confinement of optical phonons within the finite volume of the nanoparticles. This effect can be best explained using a simple model based on spatial correlation,[26–28,36] which accounts for the effects of spatial confinement of optical phonons. The phonon correlation length is infinite for a bulk crystal, which leads to the $\mathbf{q}=0$ momentum selection rule. In the case of nanoparticles, the correlation length is limited to the size of the particle, which leads to the relaxation of momentum selection rules. The Coulomb interaction, which is responsible for the LO–TO phonon splitting, weakens with decreasing particle size. Thus, the LO phonon energy is shifted towards the TO phonon energy. This qualitatively explains the softening of the LO phonons in nanoparticle systems. According to the spatial correlation model, the line shape of the first-order Raman spectrum can be given by[28]

$$I(\omega)=C\int_0^1\left[\frac{1}{[\omega-\omega_1(q)]^2+\Gamma_1^2}+\frac{1}{[\omega-\omega_2(q)]^2+\Gamma_2^2}\right]\times\exp\left(-\frac{q^2R^2}{4a^2}\right)d^3q, \tag{7}$$

where q is expressed in terms of $2\pi/a$, a is the effective lattice constant of the alloy, C is an intensity-normalization coefficient, R is the particle radius, and Γ_1 and Γ_2 are the natural linewidths of CdS and CdSe bulk crystals, respectively. $\omega_1(q)$ and $\omega_2(q)$ are the phonon dispersions for CdS- and CdSe-like LO phonons, respectively, given by[37]

$$\omega_i(q)=\omega_i(\mathrm{LO})-\Gamma_i(\mathrm{LO})\sin^2(q/4), \tag{8}$$

with $\omega_i(\mathrm{LO})$ and $\Gamma_i(\mathrm{LO})$ being the frequencies and the widths, respectively, of bulk CdS- and CdSe-like LO phonons.

By taking R as a fitting parameter along with $a=6.8$ Å, $\omega_1(\mathrm{LO})=200$, $\omega_2(\mathrm{LO})=299.5$, and $\Gamma_1(\mathrm{LO})=\Gamma_2(\mathrm{LO})=4$ cm^{-1},[23,38] Eq. (7) can be used to fit experimental line shapes of the first-order Raman spectrum. It is observed that Eq. (7) explains the shift and the high-energy-side spectral shape of the LO phonons in quite a convincing way, as shown by the dotted curve in Fig. 7(a) for the CdS-like LO phonon from the sample annealed at 550 °C. However, the low-energy-side spectral shape of the LO phonon, particularly the shoulder-like structure, cannot be fitted with Eq. (7) alone. This is due to the presence of the surface phonon modes at frequencies slightly lower than those of the optical phonons, which merge smoothly with the LO phonons on their low-frequency sides. Figure 7(b) shows similar fitting curves using Eq. (7) for the samples annealed at various temperatures, depicting a shift in the phonon frequency with annealing temperature. The dashed line in Fig. 7(b) indicates the phonon position for the bulk. Figure 8 shows the particle-size dependence of the shift in CdS-like LO phonons with respect to the bulk phonon position. The solid line in Fig. 8 is obtained from Eq. (7).

For a plane wave propagating through a crystal, the temporal and spatial variations of the wave are described in terms of the wave vector $\mathbf{k}$, which includes the square root of the dielectric constant of the semiconductor. In the frequency range between the LO and the TO phonons of a bulk material, the dielectric constant is negative, which makes $\mathbf{k}$ an imaginary quantity. Therefore, an electromagnetic wave cannot propagate in this frequency range and only surface phonons, near the surface of the crystal, decaying away from

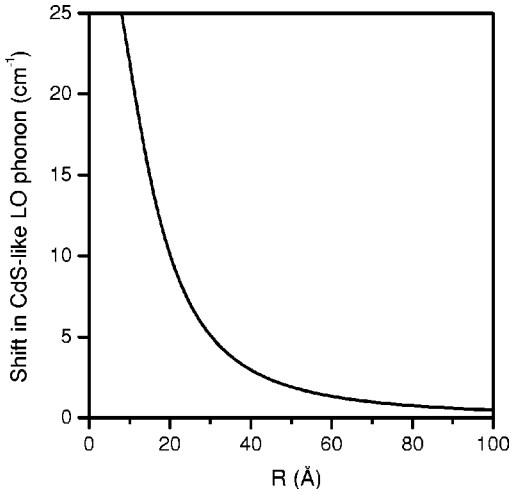

FIG. 8. Size-dependent shift in the CdS-like LO phonon as obtained from Eq. (7).

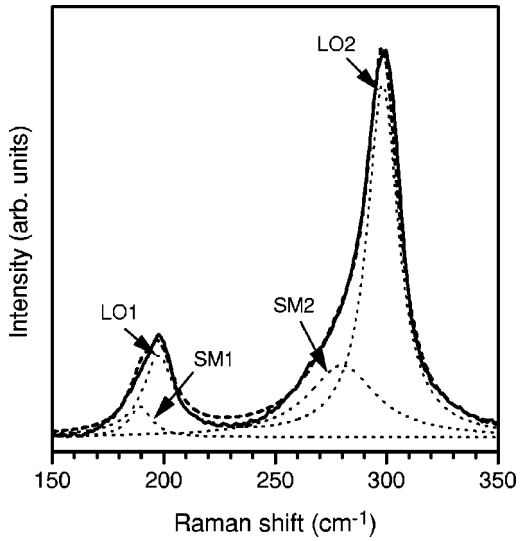

FIG. 9. LO phonons (LO1 and LO2) and the surface phonon modes (SM1 and SM2) deconvoluted from the first-order Raman spectrum presented in Fig. 6. The dotted curves show phonon contributions and the dashed line the sum of all contributions.

the surface and satisfying the boundary conditions, can exist. The frequencies of these surface phonons depend on the dielectric constants of the two media at the surface and the strengths depend on the surface-to-volume ratio of the system. These surface phonons can, therefore, be easily seen in samples containing small nanoparticles, because their surface-to-volume ratio is large. Nanoparticles can be considered as spheres of radius R, randomly distributed in a host glass matrix. For incident wavelengths $\lambda \gg R$, the electric field can be assumed to be uniform over the spheres and retardation effects can be neglected. Consequently, we can restrict the study to an isolated sphere of dielectric function $\epsilon(\omega)$, embedded in a medium with a dielectric constant ϵ_m. In the present case, ϵ_m can be assumed to be a constant because, for the amorphous glass matrix, $\epsilon_m(\omega)$ is a rather slow-varying function. In order to satisfy the boundary conditions at the interface of a nanoparticle and the glass matrix, both the electric potential and the normal component of the displacement vector must be continuous across the interface. These conditions are fulfilled for[39]

$$\epsilon(\omega) = -\epsilon_m(l+1)/l, \tag{9}$$

with $l = 1,2,3,\ldots$. The solution of Eq. (9) for $l=1$ gives the frequency of the first surface phonon mode, also known as the dipole mode or the Fröhlich mode. For $\lambda \gg R$, this is the mode which is observed in Raman spectra. The dielectric function for an alloy material can be given by[40]

$$\epsilon(\omega,x) = \epsilon_\infty(x)\left[\frac{\omega_{\mathrm{LO1}}^2(x)-\omega^2}{\omega_{\mathrm{TO1}}^2(x)-\omega^2}\right]\left[\frac{\omega_{\mathrm{LO2}}^2(x)-\omega^2}{\omega_{\mathrm{TO2}}^2(x)-\omega^2}\right], \tag{10}$$

where $\epsilon_\infty(x)$ for the CdS_xSe_{1-x} alloy can be calculated from

$$\epsilon_\infty(x) = x\epsilon_\infty^{\mathrm{CdS}} + (1-x)\epsilon_\infty^{\mathrm{CdSe}}. \tag{11}$$

By substituting the value of $\epsilon(\omega,x)$ for $x=0.65$ from Eq. (10) and then solving Eq. (9) for $l=1$, one gets the frequencies of the surface phonon modes in $CdS_{0.65}Se_{0.35}$. For $\epsilon_m = 2.25$, $\epsilon_\infty^{\mathrm{CdS}} = 5.32$, $\epsilon_\infty^{\mathrm{CdSe}} = 6.1$, $\omega_{\mathrm{LO1}} = 200$, $\omega_{\mathrm{LO2}} = 299.5$, $\omega_{\mathrm{TO1}} = 171$, and $\omega_{\mathrm{TO2}} = 258$ cm^{-1},[23,31,39,41] the calculated frequencies for the surface phonon modes come out to be $\omega_{\mathrm{SM1}} = 191.5$ and $\omega_{\mathrm{SM2}} = 279.6$ cm^{-1} for the two surface phonon modes associated with LO1 and LO2, respectively. It can be noticed from Eqs. (9) and (10) that the frequencies of the surface phonons do not depend on the size of the particle, and therefore, on the annealing temperature. Ideally, surface modes are present at the same frequency position even for the bulk, but their strengths are too small to be observed.

The first-order spectrum observed in Fig. 6 is a convolution of the surface phonon modes and the confinement-modified LO phonons. In order to extract the two contributions from the spectrum, a deconvolution was performed by considering the LO phonon line shapes of the type given by Eq. (7) with R as a fitting parameter and the surface phonon line shapes as Lorentzians. Results are presented in Fig. 9 for the sample annealed at 800 °C. The dotted lines present contributions from the surface phonons and the LO phonons, and the dashed line shows the sum of all contributions. The experimental spectral shape, shown by the solid line, can be well fitted with the theory by considering confinement effects and surface phonon modes together. The particle radius R was obtained from the fit for the samples annealed at various temperatures. The LO phonon frequencies, the particle size R, and surface phonon frequencies obtained from the deconvolution are listed in Table I, under the columns LO1, LO2, $R3$, SM1, and SM2, respectively. As expected, it can be seen from Table I that the positions of the surface phonons are independent of the particle size and are in good agreement with the calculated values of $\omega_{\mathrm{SM1}} = 191.5$ and $\omega_{\mathrm{SM2}} = 279.6$ cm^{-1}. Particle radii obtained by considering the confinement effects on the optical phonons agree well with those obtained from the PL and low-frequency Raman scattering experiments, as seen in Table I.

A close observation of the second-order Raman spectra reveals that the surface phonons are present in the 2LO phonon modes as well and also the overtones and the combination modes of the surface phonons have some trace in the second-order spectra. However, due to the comparatively

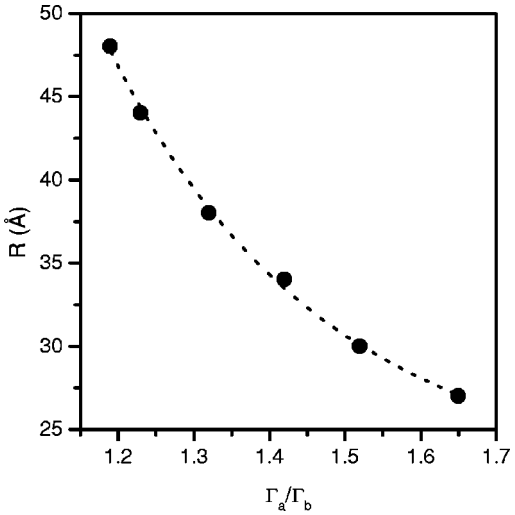

FIG. 10. Size dependence of the experimental values of the parameter Γ_a/Γ_b, which is the ratio of the half width on the low-frequency side to that on the high-frequency side of the CdS-like LO phonon. The dashed line is a guide to the eyes.

weak strengths of the second-order spectra, deconvolution was not possible within convincing error limits.

Further, apart from the asymmetry seen in the LO phonon spectral shape due to the presence of the surface phonons, Eq. (7) depicts an additional asymmetry arising from the confinement effects, which depends on the particle size. This asymmetry can be quantified by considering the parameter Γ_a/Γ_b, which is the ratio of the half widths on the low-frequency side to the high-frequency side of the peak positions of the LO phonons. As shown in Fig. 7(a), the half widths Γ_a and Γ_b can be obtained from the fit using Eq. (7) alone. Figure 10 shows the size dependence of the parameter Γ_a/Γ_b. The dashed curve in Fig. 10, which is a line to guide the eyes, gives a measure of the particle radius for a given value of the parameter Γ_a/Γ_b.

IV. CONCLUSIONS

A base glass material, in which Cd, S, and Se were introduced by diffusion, was thermally annealed to grow CdS_xSe_{1-x} nanoparticles embedded in a glass matrix. The base material does not contain any crystalline structure before annealing. As the annealing temperature was varied from 550 to 800 °C, the color of the samples changed from yellow to deep orange, indicating a continuous change in the band gap of the grown CdS_xSe_{1-x} nanoparticles. PL and Raman scattering experiments were performed on the annealed samples and an increase in particle size with increasing annealing temperature was observed. A comparative study of the confinement effects was performed using PL, low-frequency Raman scattering, and optical Raman scattering experiments. A size-dependent energy shift was observed in PL experiments. Raman experiments show shifts in low-frequency-confined acoustic phonons, and asymmetric broadening accompanied by softening of the optical phonons, in dependence on the particle size. The radii of grown particles were estimated from the three independent experimental processes using theoretical models, and were found to be in good agreement. In addition, since the surface-to-volume ratio for nanoparticles is large for our samples, the surface phonons could be observed in the optical spectral range of Raman spectra. The frequencies of the surface phonon modes are found to be in good agreement with the calculated ones and are particle-size independent.

[1] J. Warnock and D. D. Aswshalom, Phys. Rev. B **32**, 5529 (1985).
[2] H. Yukselici, P. D. Persans, and T. M. Hayes, Phys. Rev. B **52**, 11763 (1995).
[3] A. Alivasatos, J. Phys. Chem. **100**, 13226 (1996), and references therein.
[4] A. Alivasatos, Science **271**, 933 (1996).
[5] E. Menéndez-Proupin, C. Trallero-Giner, and S. E. Vlloa, Phys. Rev. B **60**, 16747 (1999).
[6] M. Rajalakshami, A. K. Arora, B. S. Bendre, and S. Mahamuni, J. Appl. Phys. **87**, 2445 (2000).
[7] A. V. Kolobov, J. Appl. Phys. **87**, 2926 (2000).
[8] A. Balandin, K. L. Wang, N. Kouklin, and S. Bandyopadhyay, Appl. Phys. Lett. **76**, 137 (2000).
[9] J. R. Huntzinger, J. Groenen, M. Cazayous, A. Mlayah, N. Bertru, C. Parantheon, O. Dehaese, H. Carrère, E. Bedel, and G. Armelles, Phys. Rev. B **61**, R10547 (2000).
[10] V. I. Klimov, A. A. Mikhailovsky, D. W. McBranch, C. A. Leatherdale, and H. G. Bawendi, Science **278**, 1011 (2000).
[11] T. Itoh, Y. Iwabuchi, and M. Kataoka, Phys. Status Solidi B **146**, 531 (1988).
[12] P. Verma, G. Irmer, and J. Monecke, J. Phys.: Condens. Matter **12**, 1097 (2000).
[13] S. Lee, J. C. Kim, H. Rho, C. S. Kim, L. M. Smith, H. E. Jackson, J. K. Furdyna, and M. Dobrowolska, Phys. Rev. B **61**, R2405 (2000).
[14] P. Verma, W. Cordts, G. Irmer, and J. Monecke, Phys. Rev. B **60**, 5778 (1999).
[15] M. Montagna and R. Dusi, Phys. Rev. B **52**, 10080 (1995).
[16] A. Tanaka, S. Onari, and T. Arai, Phys. Rev. B **47**, 1237 (1993).
[17] A. Roy and A. K. Sood, Solid State Commun. **97**, 97 (1996).
[18] T. Bischof, M. Ivanda, G. Lermann, A. Materny, and W. Kiefer, J. Raman Spectrosc. **27**, 297 (1996).
[19] L. Saviot, B. Champagnon, E. Duval, and A. I. Ekimov, Phys. Rev. B **57**, 341 (1998).
[20] A. K. Sood, J. Manendez, M. Cardona, and K. Ploog, Phys. Rev. Lett. **54**, 2111 (1985).
[21] H. B. Abel, Phys. Status Solidi B **161**, 435 (1990).
[22] A. Boukenter, B. Champagnon, E. Duval, J. L. Rousset, J. Dumas, and J. Serughetti, J. Phys. C **21**, L1097 (1988).
[23] B. Champagnon, B. Andrianasolo, and E. Duval, J. Chem. Phys. **94**, 5237 (1991).
[24] M. Fujii, T. Nagareda, S. Hayashi, and K. Yamamoto, Phys. Rev. B **44**, 6243 (1991).
[25] Y. Kayanuma, Phys. Rev. B **38**, 9797 (1988).
[26] K. K. Tiong, P. M. Amrithraj, F. H. Pollak, and D. E. Aspnes, Appl. Phys. Lett. **44**, 122 (1984).
[27] P. Verma, K. P. Jain, and S. C. Abbi, J. Appl. Phys. **79**, 3921 (1996).
[28] H. Campbell and P. M. Fauchet, Solid State Commun. **58**, 739 (1986).
[29] R. Ruppin and R. Englman, Rep. Prog. Phys. **33**, 149 (1970).
[30] H. W. Verleur and A. S. Baker, Jr., Phys. Rev. **155**, 750 (1967).
[31] See, for example, *Semiconductors–Basic Data*, edited by O. Madelung (Springer, Berlin, 1996).
[32] H. Lamb, Proc. London Math. Soc. **13**, 189 (1882).
[33] E. Duval, Phys. Rev. B **46**, 5795 (1992).
[34] R. M. Martin and L. M. Falicov, *Topics in Applied Physics* (Springer, Berlin, 1975), Vol. 8, p. 80.
[35] M. Ya Falakh, A. A. Klochikhin, and A. P. Litvinchuk, Sov. Phys. Solid State **26**, 1558 (1984).
[36] A. Roy and A. K. Sood, Phys. Rev. B **53**, 12127 (1996).
[37] H. Bilz and W. Kress, in *Phonon Dispersion Relations in Insulators* (Springer, Berlin, 1979), p. 120.
[38] A. Mlayah, A. M. Brugman, R. Carles, J. B. Renucci, M. Ya Valakh, and A. V. Pogorelov, Solid State Commun. **90**, 567 (1994).
[39] R. Fuchs and K. L. Kliewer, J. Opt. Soc. Am. **58**, 319 (1968).
[40] T. Kurosawa, J. Phys. Soc. Jpn. **16**, 1298 (1961).
[41] L. Genzel and T. P. Martin, Phys. Status Solidi B **51**, 91 (1972).